RSC Advances

PAPER

View Article Online
View Journal | View Issue

Cite this: *RSC Adv.*, 2023, **13**, 5266

Light-driven textile sensors with potential application of UV detection†

Jian Zhang,[a] Jie Zhou,[a] Qingqing Zhou,[a] Wen Wu,[a] Huanxia Zhang,[a] Xiangsong Lin,[a] Qiulan Luo,[b] Jianda Cao*[a] and Hui Ma*[a]

Received 19th October 2022
Accepted 9th January 2023

DOI: 10.1039/d2ra06607f

rsc.li/rsc-advances

Smart textiles based on monitoring systems of health conditions, structural behaviour, and external environmental conditions have been presented as elegant solutions for the increasing demands of health care. In this study, cotton fabrics (CFs) were modified by a common strategy with a dipping–padding procedure using reduced graphene oxide (RGO) and a photosensitive dye, spiropyran (SP), which can detect environmental UV light. The morphology of the CF is observed by scanning electron microscopy (SEM) measurements showing that the topography structure of coatings is related to the SP content. The resistance of the textile sensors decreases after UV radiation, which may be attributed to the easier electron transmission on the coatings of the CF. With the increase of SP content, the introduction of a large amount of SP within the composites could cause discontinuous distributions of RGO in the fiber surfaces, preventing electron transmission within the coatings of the RGO. The surface wettability of the coatings and the sweat sensitivity are also studied before and after UV radiation.

Introduction

Smart textiles with the ability to monitor health conditions, structural behavior, and external environmental conditions have received increasing interest in the demands of health care.[1–4] Numerous smart materials and specific structures have been developed to promote new technology in intelligent sensing fields.[5–9] For instance, stimuli-responsive materials combined with textile fabrics have drawn considerable attention because of the property of sensing, convenient human–computer interaction, smart devices with performing data sensing, and self-adaptation.[7–9] The application of smart textiles has experienced rapid growth these years.[10–12] In particular, these smart textiles can sense environmental conditions or external stimuli, such as movement, sweetness, light, pH, temperature, pressure, mechanical or magnetic effects and electricity.[13–17] Smart textile fabrics can even release drugs and moisture simultaneously transferred to the skin, assisting in modulating the energetic behavior during movements.[18] Smart textiles can also change color, light up in special patterns, or even display videos.[19,20] Many of the above materials are prepared using graphene because graphene is resistant to temperature and chemical agents. In particular, the excellent conductivity and rich chemical properties of the surface make it an ideal material to adhere to textile surfaces.[21–23] Therefore, graphene-based smart materials have been widely and extensively used in smart textiles.

The resistance change of graphene oxide (GO) induced by electron transmission can be detected, which could sense the environmental factors. Zhen *et al.* developed wearable textile strain sensors with reduced graphene oxide (RGO). The GO coatings of the textile acted as a colorant dye of the polyester fabric, endowing the strain sensor of the textile with excellent performance.[24] Cao *et al.* fabricated a wearable type of flexible textile sensor using RGO-Ag nanowire cotton fiber.[25] The addition of Ag nanowire provided a fast electron transmission, resulting in a significantly improved property and the high sensitivity increased from 0.084 to 4.23 kPa^{-1}. Hao Tian *et al.* demonstrated a facile method to create RGO micro ribbons. The textile sensors can experience resistance changes responding to moisture adsorption from human breaths.[26] As discussed above, the wearable and flexible electronic fabric sensors by RGO have enormous potential applications and are expected to be further explored in environmentally responsive studies.[27–30]

Smart textiles respond to external stimuli quickly with adequate responsiveness, which is prone to enhance their protective purpose.[31–33] It is well known that the harmful effects of accumulative exposure to UV radiation may be related to sunburn, skin cancer, premature aging, and even suppression of the immune system. An easy way to utilize UV sensors would help people to take exact protection according to the amount of environmental UV radiation.[34,35] While previously reported textile sensors are focused on color change without quantitative

[a]*Key Laboratory of Yarn Materials Forming and Composite Processing Technology of Zhejiang Province, College of Material and Textile Engineering, Jiaxing University, Jiaxing, 314001, China. E-mail: mahone1136@163.com*

[b]*College of Fashion and Design, Jiaxing Nanhu University, Jiaxing 314001, Zhejiang, China*

† Electronic supplementary information (ESI) available. See DOI: https://doi.org/10.1039/d2ra06607f

analysis of the UV radiation. It is possible to combine the UV-responsive materials and RGO to perceive and record the UV strength by converting light signals into electrical signals.

The UV-sensitive spiropyran (SP) changed to merocyanine (MC) under UV radiation, could be used to reflect the UV radiation conditions. In this work, a simple and effective method is utilized to prepare UV-sensitive textiles in the industry. Based on π–π conjugation, SP molecules and RGO are assembled to the cotton fibers (CF) to prepare the smart fabrics. The SP molecules are anchored on the surface of graphene nanosheets which could sense the UV radiation by breaking the –C–O– covalent bond, resulting in the resistance change of the textile sensors. Scanning electron microscopy (SEM) and X-ray photoelectron spectroscopy (XPS), and X-ray diffraction analysis (XRD) measurements are taken to characterize the surface properties of the textile sensors. In addition, the sensitivity of the fabrics to artificial sweat was evaluated in detail, and the mechanism of the specific response of the textile sensors to UV radiation is also clarified.

Results and discussion

Morphology and composition analysis of RGO/SP@Cotton composites

The new generation of composites on the CF surface is combined by GO and a certain amount of SP. Fig. 1 shows the morphology before and after surface modification analyzed by SEM images. Some pollutant particles are attached to the surface of the original, unmodified CF showing that the surface is not completely smooth. After modification with a certain amount of RGO (Fig. 1b), a layer of disordered RGO covered the surface of CF. Some parts of the modified fiber surface are coated in an orderly manner, while some parts have defects and protrusions resulting from the agglomeration and hardening phenomenon of RGO (Fig. 1b). The carboxylate groups of the GO cause the GO dispersed uniformly in water by the electrostatic repulsion force, while the graphene nanosheets are stacked in a disordered pattern of the surface of CF during the dipping–padding procedures that may arise from the electrostatic repulsion effect by various numbers of carboxylate groups of GO.

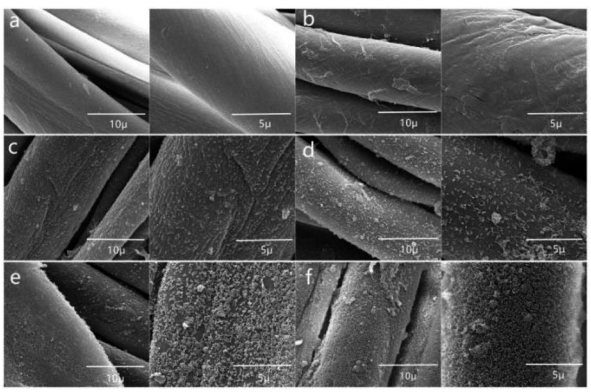

Fig. 1 The SEM images with RGO/SP composites modified CF, (a–f) were as follows: CF, RGO/SP-0, RGO/SP-10, RGO/SP-20, RGO/SP-30, and RGO/SP-40.

In Fig. 1c, the RGO/SP layer coated on the fiber surface becomes ordered and homogeneous with the SP content increasing from 0 to 10%. When the SP molecules are adsorbed onto the GO surfaces by π–π interactions between graphene nanosheets and SP molecules, the graphene nanosheets are stacked in an ordered state resulting in ordered distribution on the surface of the fibers at macro levels. Thus, when the SP molecules are introduced onto GO surfaces, the π–π interactions between SP and graphene nanosheets cause the SP molecules to be fixed at the surfaces of graphene nanosheets, thereby decreasing the repulsion forces due to the increase of hydrophobic interactions between the RGO/SP composites. These hydrophobic forces cause the composites orderly to coat on the surfaces of CF by decreasing the hydration strength of the GO nanosheets, thereby inducing a preference for orderly coating rather than a random stacking state. Thus, the coating on the CF shows good homogeneity.

Fig. S1† shows Raman spectra of GO/SP-0, GO/SP-10, and GO/SP-10 after UV radiation. It is confirmed the D ($\sim$1350 cm^{-1}) and the G ($\sim$1600 cm^{-1}) bands are the characteristic peaks of the RGO fabricated by the method of Hummers.[36,37] The SPs are combined with RGO by noncovalent bonding, so the crystal structure of RGO would remain in its original state. The baseline of the RGO/SP-10 Raman spectrum rose and became broad after UV radiation, which is due to the fluorescence of MC molecules converted from SP by UV radiation. XPS and XRD were used to detect the chemical composition of textile surfaces before and after modification. As shown in Fig. S2 and S3,† the N element appeared on the surface of the textile in the GO/SP-10 and the XRD patterns of GO/SP-10 exhibit sharper and left shift, showing that the SPs were introduced to the textile surface.

The introduction of a large amount of SP within the composites could cause protrusion and wrinkle structures in the fiber surfaces (Fig. 1d–f). Nevertheless, when the proportion of SP increases to a certain extent, the composites coating begins to show a small amount of inhomogeneity on the surface of CF (Fig. 1d). When the proportion of SP increases from 30% to 40%, the wrinkle structure could be observed on the surface of the CF, which may be caused by the aggregation of RGO/SP composites and the SP molecules when the SP corporation is relatively high (Fig. 1e and f). Furthermore, the electron transmission is weakly hindered within the RGO of the regular composite coatings which may strongly respond to UV radiation resulting from the regular RGO stacking formation.

UV responsive properties

Photochromic dyes alter the structure to absorb radiation in response to optical stimulation.[38] The photo-induced transformations can be exploited to modulate the resistance of the CF. In Fig. 2, the resistance performances of CF with RGO/SP-1, RGO/SP-20, RGO/SP-30, and RGO/SP-40 are smaller, while the resistance of RGO/SP-10 significantly changes compared with other SP contents. As discussed in Fig. 1, the surface

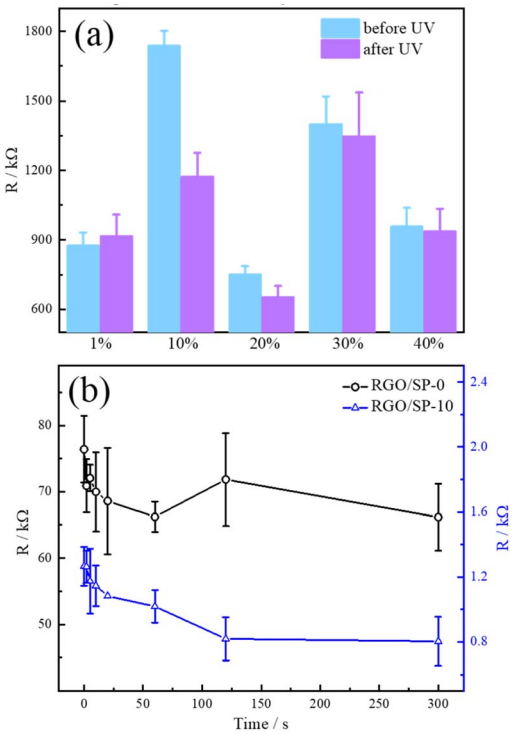

Fig. 2 (a) The resistance of the textile sensor as a function of SP content before and after UV radiation. (b) The resistance of the RGO/SP-0 and RGO/SP-10 composites modified textile as a function of UV radiation time.

morphology of the CF with RGO/SP-10 is regular and the graphene nanosheets are stacked with a thicker lamellar structure. The electron transmission is changed before and after UV radiation with the regular coatings. When the SP content is low (1%), the SP structure change within the coatings is not sufficient to change the arrangement of graphene nanosheets. While the SP contents are increased to 20%, 30%, and 40%, the continuity of the graphene nanosheets was disturbed at high SP contents resulting in the sensitivity decrease of the CF.

As shown in Fig. 2, the resistance of the RGO/SP composites modified CF changes under the condition of UV radiation. Furthermore, it is necessary to detect how the resistance of the smart textiles behaves as a function of UV radiation time because the UV radiation will continue for a long time under some realistic circumstances. In Fig. 2b, the resistance of the CF modified by RGO remains almost at a constant value as a function of time, while the resistance of the CF coated with RGO/SP-10 composites decreases with the increase of UV radiation time. The stacked structure of RGO/SP-0 is insensitive to UV light arising from the RGO/SP-0 coatings are independent of UV radiation. The resistance is unchanged over the UV radiation process. However, when the covalent bond within the SP molecules between the carbon and oxygen atoms breaks, the SP molecular configuration changes, resulting in ion pairs and a planar conjugation structure formed under UV light. The number of ion pairs and planar conjugation structures increases with the increase of UV radiation time until the breaking and reuniting of the –C–O covalent bond reaches a steady-state equilibrium stage. Thus, the tighter stack structure of the coating favors the directional transmission of electrons on the surface of the textile.

The SP dye molecule is well known for its suitable photochromic property and reversible manner by UV-visible radiation.[39] As illustrated in Fig. 2, the breaking of the –C–O covalent bond contributed to the resistance change of the smart textile under UV radiation. In other words, the molecular configuration and polarity are changed compared with the original SP molecules (Fig. 3). Therefore, the $-N^+$ and $-O^-$ groups within the SP molecule are generated after the breaking of the –C–O covalent bond. Thus, the dipole–dipole interactions between different ionic pairs tighten the spacing of two graphene nanosheets. Meanwhile, $-N^+$ in one SP molecule will be attracted by $-O^-$ in another SP molecule which will also cause the spacing of the graphene nanosheet to become smaller resulting in a resistance decrease in the CF. The resistance change of the smart textile under UV radiation shows a potential means of recording by the UV circumstance.

Density-functional theory (DFT) has been performed as a theoretical method to study the isomerization reaction under UV radiation.[40] The reaction process of SP to MC mainly involves the cleavage of the weaker –C–O bond, followed by the change of molecule configuration, the opening of the six-membered ring system in SP, and the generation of the conjugated MC isomers (Fig. S4†). It turns out that the *cis*-MC isomer is energetically unstable and tends to transform into another *trans*-MC isomer with a lower energy value. In other words, the *cis*-MC isomer rotates by twisting the dihedral angle around the center finally producing the *trans*-MC isomer to form a more stable state. The *cis*-MC isomer has non-planar geometric structures, while the *trans*-MC isomer has planar conjugation structures. The newly formed *trans*-MC isomer is like a bridge connecting various GRO nanosheets (Fig. S5†). Therefore, the resistance of the RGO/SP composites modified CF decreases under UV radiation.

Artificial sweat response before and after UV radiation

When exposed to a natural environment, the sweat solution of humans may affect the resistance of the CF because the ions in the sweat solution could specifically interact with the newly formed $-N^+$ and $-O^-$ groups. Thus, it is necessary to study the sweat effects on resistance behavior. It is well known that the ions can form various strengths of ion pairs according to

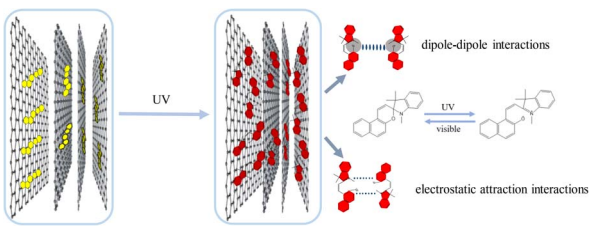

Fig. 3 Schematic illustration of SP structure and the RGO/SP coatings change based on light-driven.

Collin's role of the law of matching water affinities (LMWA).[41,42] So the various strength of ion pairs can be used to make fabric sensors sweat-responsive.

As discussed above, the –C–O covalent bond within the SP molecules breaks under UV radiation. The various hydration strength of ions specifically interacts with the newly formed $–N^+$ and $–O^-$ groups. In other words, the tight ion pairs strongly bind the ions resulting in a low rate of directional movement. While for the loose ion pairs, the directional movement of the ions becomes easy compared with the tight ion pairs, leading to the low resistance of the textile sensors. Furthermore, the surface polar property increases by the newly formed $–N^+$ and $–O^-$ groups under UV radiation. So the hydration strength of the textile sensors increases and the interactions between water molecules and the textile sensors elevate, contributing to the easy directional ion transition and a higher number of ion channels within the textile sensors. Thus, the resistance of the textile is synergistically regulated by the ion pairs of the $–N^+$ and $–O^-$ groups with various ions and the electron transmission within the RGO nanosheets.

As shown in Fig. 4, the resistance of the textile decreases under the condition of UV radiation in the artificial sweat of pH 4.5 and 8.0. The tight and loose ion pairs are dominated by $–N^+$ and $–O^-$ groups of SP and the counterions that can regulate the ion movement on the surface, thereby increasing the resistance. Furthermore, the polar property increases under UV radiation leading to the extendibility of infiltration degree attributed to the easier ion movement and the decrease in the resistance of the textile sensor.

The electrostatic interactions between $–N^+$ and $–O^-$ groups, and the ions in artificial sweat decrease the electrostatic attraction between the cation $–N^+$ and anion $–O^-$ groups. That is, the competitive adsorption of counterions increases the resistance of ion movement leading to the increase in the resistance of the textile sensor. According to different interactions within the textile sensors, the extendibility of infiltration degree induces the spreading liquid phase on the surface of the textile sensor, which plays a dominant role in the decrease in the resistance of the textile sensor driven by more ion channels formed within the lamellar spacing of RGO. Thus, this new light-responsive textile may be more likely to be applied in light and sweat-responsive textile sensors. Here, the lamp is utilized to show the resistance decrease of the CF by light strength increase under UV radiation (Fig. 4b). Likewise, it is expected that the digital output device could be potentially used to record the resistance performance of the textile sensors which is related to the UV circumstance.

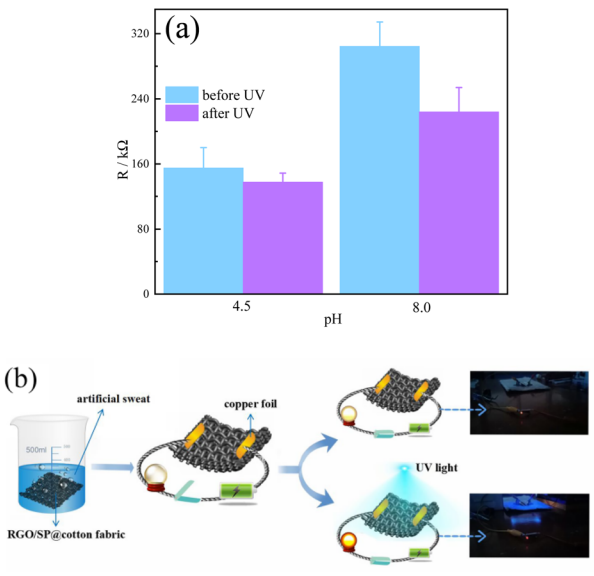

Fig. 4 (a) Resistance change of the textile sensors before and after UV radiation in the artificial sweet solution. (b) The light strength of the lamp under UV radiation in the artificial sweat solution.

Wettability of the textile sensor before and after UV radiation

Direct observation of wettability change may provide insights into the strength of UV radiation. In Fig. 5, the wettability of the RGO/SP-0 textile sensor remains unchanged while the wettability of RGO/SP-10 coatings decreases under UV radiation. The structure and polar properties of RGO/SP-0 coatings are unchanged under UV radiation, so the contact angle of the textile sensor is a constant value before and after UV radiation. While as for the RGO/SP-10 coatings on the textile sensor, the SP molecules are neutral before UV radiation leading to the interactions being weak between the coatings and water, so the contact angle is large.

The interactions between the $–N^+$ and $–O^-$ groups and water increases result in a decrease in contact angle, demonstrating that the wettability increases under UV radiation. The contact angle of the coatings on the textile increases with the increased SP content (Fig. 5). The contact angle should also increase with the roughness increase of the coatings on the textile sensor by the Lotus effect.[43,44] While in Fig. 5, the contact angle of the RGO/SP-10 coatings on the textile sensor is larger than the RGO/SP-0 coatings, which implies that the roughness of the coatings plays a dominant role in the wettability of the textile sensors. Compared with the contact angle of RGO/SP-10 coatings before and after UV radiation, the small change shows that SP content is too low in the RGO/SP-10 composite to change the surface

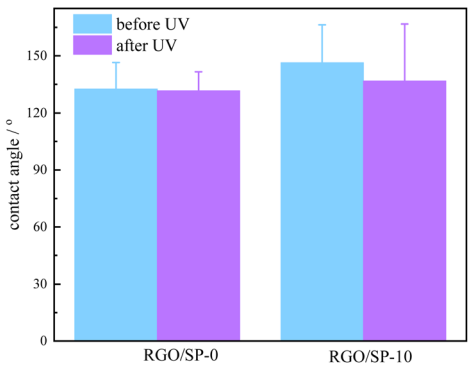

Fig. 5 The wettability change of RGO and RGO/SP-10 textile sensors before and after UV radiation.

tension of the textile sensor under UV radiation, which leads to a weak influence on the surface wettability.

Experimental

Materials

Cotton fabrics (CF) (plain fabric, 80 g m^{-2}) were purchased from Hua Fang Co., Ltd, and cleaned by ultrasonic with deionized water, acetone and ethanol for ~30 min respectively and dried in the oven. Spiropyran (SP) was obtained from TCI (Shanghai) Development Co., Ltd. Hydrazine monohydrate (~85%), H_2SO_4 (98.0%), $NaNO_3$ (≥99.0%), H_2O_2 (≥30.0%), $KMnO_4$ (≥99.5%) and graphite powder (≥99.85%) were purchased from Sinopharm Chemical Reagent Co., Ltd. All the chemical reagents were used as received without purification. The water used here was purified by filtration, giving a resistivity of 18.2 MΩ cm. Graphene oxide (GO) was synthesized by the method of Hummers.[45]

Fabrication of RGO/SP composites

A certain amount of SP was mixed with freeze-dried GO powder in different mass proportions (0 : 100, 1 : 99, 10 : 90, 20 : 80, 30 : 70, 40 : 60) and ground for ~1 h. Then the above-mixed powders were prepared into ~0.2% solution and ultrasonic for about ~1 h.[46,47] Afterward, five pieces of 5 × 10 cm^2 CFs were dipped in the GO/SP composites solution for ~10 min, and then passed through a two-roll laboratory padder (0.2 MP, 1.5 m min^{-1}) (Fig. 6). The above dipping–padding procedures were repeated 5 times, and the as-prepared fabrics were dried at 60 °C in the oven, after that the CF were reduced in hydrazine hydrate solutions at 90 °C for ~3 h. Finally, prepared CF were washed with deionized water and then dried under 60 °C before use. The as-prepared CF are labeled as RGO/SP@CF-0, RGO/C_{60}@CF-1, RGO/SP@CF-10, RGO/SP@CF-20, RGO/SP@CF-30, and RGO/SP@CF-40, respectively.

Characterizations

The surface morphology of the CF was observed by scanning electron microscope (SEM, Quanta 400F). The UV absorption spectrophotometry was shown in Fig. S6† and the 365 nm was adopted in this work. The resistivity of CF was conducted by International Electro Technical Commission Procedure 93-1980 (Fig. S7†), and the resistivity of the sensors was calculated by the equation:

$$R_s = R\,L/d \quad (1)$$

where R_s, R, d, L were the surface resistivity of fabrics (Ω), the resistance of the fabrics (Ω), the distance between two parallel electrodes (cm), the effective length of the specific electrode (cm), respectively. All the resistivity of the fabrics mentioned in this article was surface resistivity. The water contact angles on the surface of CF were determined using a contact angle goniometer (Krüss, Drop Shape Analyzer Series) at ~25 °C.

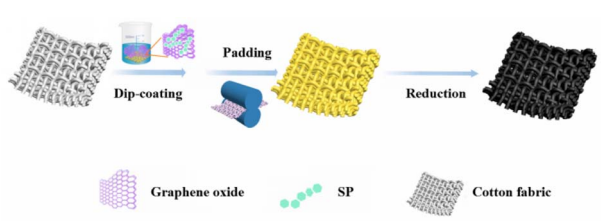

Fig. 6 Schematic diagram of the UV-sensitive sensors prepared by the industrial method.

Conclusions

In this work, RGO/SP coatings with light and ion sensing functions were prepared through industrial dipping–padding and chemical reduction methods. The prepared RGO coatings had no response to UV light and various solutions. While RGO/SP-10 coatings had good responsiveness to UV radiation and different sweat solutions, the –C–O covalent bond broke under UV radiation leading to a resistance decrease. When the SP content is low, the resistance is almost unchanged under UV radiation. The RGO/SP-10 coatings on the textile sensor have distinct resistance performance before and after UV radiation, which may be applied in light-responsive textile sensors. The fabric-based UV sensors also exhibited different artificial sweat responses and wettability under UV radiation. The resistance of the textile decreases under of UV radiation in the artificial sweat, which may be driven by more ion channels formed within the lamellar spacing of RGO. This work provides fundamental insights into the role of RGO/SP in light sensing and inspires the design of the next generation of sensitive and highly flexible intelligent ion sensors.

Conflicts of interest

There are no conflicts to declare.

Acknowledgements

This work is supported by the Natural Science Foundation of Zhejiang Province (LY21E030018), Open Project Program of Key Laboratory of Yarn Materials Forming and Composite Processing Technology of Zhejiang Province (MTC-2020-25), Open Research Program of Jiaxing University (JJ20220012), and Jiaxing Research and Development Program (2022AY10014).

Notes and references

1 A. Singh, A. Sharma and S. Arya, Human sweat-based wearable glucose sensor on cotton fabric for real-time monitoring, *J. Anal. Sci. Technol.*, 2022, **13**, 1–13.
2 A. Sharma, A. Singh, V. Gupta and S. Arya, Advancements and future prospects of wearable sensing technology for healthcare applications, *Sens. Diagn.*, 2022, **1**, 387–404.
3 S. Kurasawa, H. Ishizawa, K. Fujimoto, S. Chino and S. Koyama, Development of smart textiles for self-monitoring blood glucose by using optical fiber sensor, *J. Fiber Sci. Technol.*, 2020, **76**, 104–112.

4 A. Singh, A. Sharma, A. Ahmed and S. Arya, Highly selective and efficient electrochemical sensing of ascorbic acid via CuO/rGO nanocomposites deposited on conductive fabric, *Appl. Phys. A*, 2022, **128**, 1–12.
5 S. P. Hargunani, R. P. Sonekar, A. Singh, A. Khosla and S. Arya, Structural and spectral studies of Ce3+ doped Sr3Y (BO3) 3 nano phosphors prepared by combustion synthesis, *Mater. Technol.*, 2022, **37**, 450–461.
6 A. Singh, S. Arya, M. Khanuja, A. K. Hafiz, R. Datt, V. Gupta and A. Khosla, Eu doped NaYF4@ Er: TiO2 nanoparticles for tunable ultraviolet light based anti-counterfeiting applications, *Microsyst. Technol.*, 2020, 295–304.
7 X. Wang, Z. Liu and T. Zhang, Flexible sensing electronics for wearable/attachable health monitoring, *Small*, 2017, **13**, 1602790.
8 N. Testoni, C. Aguzzi, V. Arditi, F. Zonzini, L. De Marchi, A. Marzani and T. S. Cinotti, A sensor network with embedded data processing and data-to-cloud capabilities for vibration-based real-time SHM, *J. Sens.*, 2018, **2018**, 1–12.
9 O. Ojuroye, R. Torah, S. Beeby and A. Wilde, *Smart textiles for smart home control and enriching future wireless sensor network data*, Springer International Publishing, 2017, pp. 159–183.
10 J. Ren, C. Wang, X. Zhang, T. Carey, K. Chen, Y. Yin and F. Torrisi, Environmentally-friendly conductive cotton fabric as flexible strain sensor based on hot press reduced graphene oxide, *Carbon*, 2017, **111**, 622–630.
11 O. Atalay, A. Atalay, J. Gafford and C. Walsh, A Highly sensitive capacitive-based soft pressure sensor based on a conductive fabric and a microporous dielectric layer, *Adv. Mater. Technol.*, 2018, **3**, 1700237.
12 S. J. Kim, W. Song, Y. Yi, B. K. Min, S. Mondal, K. S. An and C. G. Choi, High durability and waterproofing rGO/SWCNT-fabric-based multifunctional sensors for human-motion detection, *ACS Appl. Mater. Interfaces*, 2018, **10**, 3921–3928.
13 S. Hu, M. Dai, T. Dong and T. Liu, A textile sensor for long durations of human motion capture, *Sensors*, 2019, **19**, 2369.
14 E. Guido, G. Rosace, V. Re, M. Caldara and C. Colleoni, Optical monitoring of sweat pH by a textile fabric wearable sensor based on covalently bonded litmus-3-glycidoxypropyltrimethoxysilane coating, *Sens. Actuators, B*, 2016, **222**, 213–220.
15 D. Kim, K. Keum, G. Lee, D. Kim, S. S. Lee and J. S. Ha, Flexible, water-proof, wire-type supercapacitors integrated with wire-type UV/NO_2 sensors on textiles, *Nano Energy*, 2017, **35**, 199–206.
16 M. L. Zamora, J. M. Dominguez, R. M. Trujillo, C. B. Goy, M. A. Sanchez and R. E. Madrid, Potentiometric Textile-Based pH Sensor, *Sens. Actuators, B*, 2018, **260**, 601–608.
17 R. Wu, L. Ma, C. Hou, Z. Meng and X. Y. Liu, Silk composite electronic textile sensor for high space precision 2D combo temperature–pressure sensing, *Small*, 2019, **15**, 1901558.
18 X. Wang, H. Hu, Z. Yang, L. He, Y. Kong, B. Fei and J. H. Xin, Smart hydrogel-functionalized textile system with moisture management property for skin application, *Smart Mater. Struct.*, 2014, **23**, 125027.
19 K. Cherenack, C. Zysset, T. Kinkeldei, N. Münzenrieder and G. Tröster, Woven electronic fibers with sensing and display functions for smart textiles, *Adv. Mater.*, 2010, **22**, 5071.
20 Q. Shi, J. Sun, C. Hou, Y. Li and H. Wang, Advanced functional fiber and smart textile, *Adv. Fiber Mater.*, 2019, **1**, 3–31.
21 G. M. N. Islam, M. A. Ali and S. Collie, Textile sensors for wearable applications: a comprehensive review, *Cellulose*, 2020, **27**, 6103–6131.
22 D. Du, P. Li and J. Ouyang, Graphene coated nonwoven fabrics as wearable sensors, *J. Mater. Chem. C*, 2016, **4**, 3224–3230.
23 B. Yin, Y. Wen, T. Hong, Z. Xie, G. Yuan, Q. Ji and H. Jia, Highly stretchable, ultrasensitive, and wearable strain sensors based on facilely prepared reduced graphene oxide woven fabrics in an ethanol flame, *ACS Appl. Mater. Interfaces*, 2017, **9**, 32054–32064.
24 Y. Zhen, P. Yu, H. Xiao-Lin, Y. Yifan, L. Jiang, J. Muqiang, Z. Yingying, Y. Yi and R. Tian-Ling, Graphene textile strain sensor with negative resistance variation for human motion detection, *ACS Nano*, 2018, **12**, 9134–9141.
25 M. Cao, M. Wang, L. Li, H. Qiu, M. A. Padhiar and Z. Yang, Wearable rGO-Ag NW@cotton fiber piezoresistive sensor based on the fast charge transport channel provided by Ag nanowire, *Nano Energy*, 2018, **50**, 528–535.
26 H. T. H. Shi, S. Jang and H. E. Naguib, A freestanding laser-assisted reduced graphene oxide micro-ribbon textile electrode fabricated on liquid surface for supercapacitors and breath sensors, *ACS Appl. Mater. Interfaces*, 2019, **11**, 27183–27191.
27 H. Cheng, Z. Dong, C. Hu, Y. Zhao, Y. Hu, L. Qu, C. Nan and L. Dai, Textile electrodes woven by carbon nanotube–graphene hybrid fibers for flexible electrochemical capacitors, *Nanoscale*, 2013, **5**, 3428–3434.
28 Y. Liu, L. Xia, Q. Zhang, H. Guo, A. Wang, W. Xu and Y. Wang, Structure and properties of carboxymethyl cotton fabric loaded by reduced graphene oxide, *Carbohydr. Polym.*, 2019, **214**, 117–123.
29 R. Xu, Y. Lu, C. Jiang, J. Chen, P. Mao, G. Gao, L. Zhang and S. Wu, Facile fabrication of three-dimensional graphene foam/poly(dimethylsiloxane) composites and their potential application as strain sensor, *ACS Appl. Mater. Interfaces*, 2014, **6**, 13455–13460.
30 S. Ling, Q. Wang, D. Zhang, Y. Zhang, X. Mu, D. L. Kaplan and M. J. Buehler, Integration of stiff graphene and tough silk for the design and fabrication of versatile electronic materials, *Adv. Funct. Mater.*, 2018, **28**, 189–198.
31 M. Vikova and M. Vik, Alternative UV sensors based on color-changeable pigments, *Adv. Chem. Eng. Sci.*, 2011, **1**, 224–230.
32 S. Roy, Impact of UV Radiation on genome stability and human health, *Adv. Exp. Med. Biol.*, 2017, 207–219.
33 S. L. Yu and S. K. Lee, Ultraviolet radiation: DNA Damage, repair, and human disorders, *Mol. Cell. Toxicol.*, 2017, **13**, 21–28.
34 L. Liu, Y. Ren, J. Pan, Z. Liu and F. Yan, Printable UV-Light sensor for human eye protection, *ACS Appl. Mater. Interfaces*, 2019, **12**, 1495–1503.

35 G. Y. Chen and W. Zilong, Towards extremely sensitive ultraviolet-light sensors employing photochromic optical microfiber, *J. Sens.*, 2015, **2015**, 586318.
36 D. Marcin Behunová, G. Gallios, V. Girman, H. Kolev, M. Kaňuchová, S. Dolinská and M. Václavíková, Electrophoretic deposition of graphene oxide on stainless steel substrate, *J. Nanomater.*, 2021, **11**, 1779.
37 N. Chadha, R. Sharma and P. Saini, A new insight into the structural modulation of graphene oxide upon chemical reduction probed by raman spectroscopy and X-ray diffraction, *J. Carbon Lett.*, 2021, **31**, 1125–1131.
38 R. Evans, T. Hanley, M. Skidmore, T. Davis, G. Such, L. Yee, G. Ball and D. Lewis, The generic enhancement of photochromic dye switching speeds in a rigid polymer matrix, *Nat. Mater.*, 2005, **4**, 249–253.
39 R. Klajn, Spiropyran-based dynamic materials, *Chem. Soc. Rev.*, 2013, **43**, 148–184.
40 M. Valiev, E. J. Bylaska, N. Govind, K. Kowalski, T. P. Straatsma, H. J. J. Van Dam, D. Wang, J. Nieplocha, E. Aprà and T. L. Windus, NWChem: a comprehensive and scalable open-source solution for large scale molecular simulations, *J. Comput. Phys. Commun.*, 2010, **181**, 1477–1489.
41 K. D. Collins, Ions from the hofmeister series and osmolytes: effects on proteins in solution and in the crystallization process, *Methods*, 2004, **34**, 300–311.
42 K. D. Collins, Ion hydration: implications for cellular function, polyelectrolytes, and protein crystallization, *Biophys. Chem.*, 2006, **119**, 271–281.
43 M. Yamamoto, N. Nishikawa, H. Mayama, Y. Nonomura and S. Yokojima, Theoretical explanation of the lotus effect: superhydrophobic property changes by removal of nanostructures from the surface of a lotus leaf, *Langmuir*, 2015, **31**, 7355–7363.
44 A. Marmur, The lotus effect: superhydrophobicity and metastability, *Langmuir*, 2004, **20**, 3517–3519.
45 L. Cui, P. Zhang, Y. Xiao, Y. Liang, H. Liang, Z. Cheng and L. Qu, High rate production of clean water based on the combined photo-electro-thermal effect of graphene architecture, *Adv. Mater.*, 2018, **30**, 1706805.
46 V. Georgakilas, J. N. Tiwari, K. C. Kemp, J. A. Perman, A. B. Bourlinos, K. S. Kim and R. Zboril, Noncovalent functionalization of graphene and graphene oxide for energy materials, biosensing, catalytic, and biomedical applications, *Chem. Rev.*, 2016, **116**, 5464–5519.
47 X. Zhang, L. Hou and P. Samorì, Coupling carbon nanomaterials with photochromic molecules for the generation of optically responsive materials, *Nat. Commun.*, 2016, **7**, 1–14.